Journal of Applied Electrochemistry (2020) 50:217–230
https://doi.org/10.1007/s10800-019-01392-1

RESEARCH ARTICLE

Mineralization of cyanide originating from gold leaching effluent using electro-oxidation: multi-objective optimization and kinetic study

Izabela Dobrosz-Gómez[1] · Miguel Ángel Gómez García[2] · Guillermo H. Gaviria[2] · Edison GilPavas[3]

Received: 24 August 2019 / Accepted: 16 December 2019 / Published online: 3 January 2020

Abstract

This study examines the electro-oxidation (EO) of cyanide originating from an industrial plant´s gold leaching effluent. Experiments were carried out in a laboratory-scale batch cell reactor. Monopolar configuration of electrodes consisting of graphite (anode) and aluminum (cathode) was employed, operating in galvanostatic mode. Response Surface Methodology (RSM), based on a Box–Behnken experimental Design (BBD), was used to optimize the EO operational conditions. Three independent process variables were considered: initial cyanide concentration ($[CN^-]_0 = 1000–2000$ mg L^{-1}), current density ($J = 7–107$ mA cm^{-2}), and stirring velocity ($\eta = 250–750$ rpm). The cyanide conversion $\left(X_{CN^-}\right)$, Chemical Oxygen Demand (COD) removal percentage ($\%R_{COD}$), and specific Energy Consumption per unit mass of removed cyanide (EC) were analyzed as response variables. Multi-objective optimization let to establish the most effective EO conditions ($[CN^-]_0 = 1000$ mg L^{-1}, $J = 100$ mA cm^{-2} and $\eta = 750$ rpm). The experimental data (X_{CN^-}, $\%R_{COD}$, and EC) were fitted to second-order polynomial models with adjusted correlation coefficients (R^2_{adj}) of ca. 98, 99 and 87%, respectively. The kinetic analysis, performed at optimal EO operational conditions, allowed determination of time required to meet Colombian permissible discharge limits. The predictive capacity of kinetic expressions was verified against experimental data obtained for gold leaching effluent. Total cyanide removal and 96% of COD reduction were obtained, requiring EC of 71.33 kWh kg^{-1} and 180 min. The BOD_5 (biological oxygen demand)/COD ratio increased from 4.52×10^{-4} to 0.5573, confirming effluent biodegradability after EO treatment.

Electronic supplementary material The online version of this article (https://doi.org/10.1007/s10800-019-01392-1) contains supplementary material, which is available to authorized users.

Extended author information available on the last page of the article

Graphic Abstract

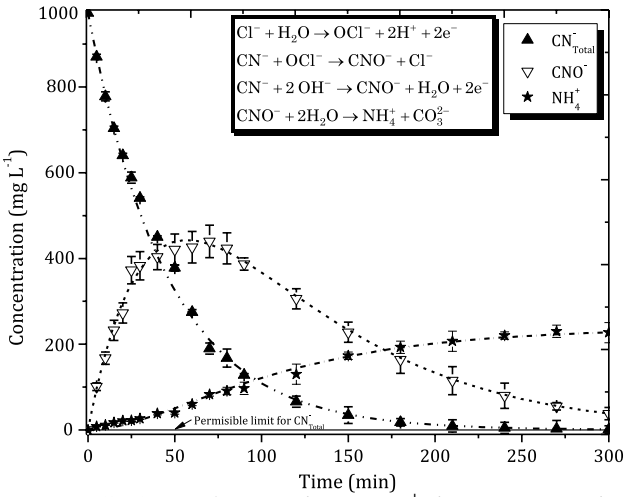

The variation of cyanide (CN^-), cyanate (CNO^-) and ammonium (NH_4^+) ions concentrations vs. time at alkaline conditions. EO operational conditions: $[CN^-]0 = 1000$ mg/L, $J = 100$ mA/cm^2 , $\eta = 750$ rpm, [NaCl] = 0.15 M and pH 11.1.

Keywords Cyanide · Electrochemical oxidation · Gold leaching effluents · Optimization · Kinetic study

1 Introduction

Many industrial processes (plastic, textile, electroplating, galvanized, metallurgical, pharmaceutical, agricultural, cosmetics and precious metal mining) use cyanide as a principal chemical [1]. Hydrocyanic acid (HCN) and potassium and/or sodium cyanide salts (v.g., KCN or NaCN) are the main human-made cyanide products. The later (NaCN) is the most common chemical in gold and silver mining initiatives. During the cyanidation process (Eq. 1), and in the presence of oxygen and under alkaline conditions, cyanide solutions dissolve precious metals from their ores [2]:

$$4Au + 8NaCN + O_2 + H_2O \rightarrow 4Na\left[Au(CN)_2\right] + 4NaOH \quad (1)$$

Although gold leaching can be performed using solutions with relatively low cyanide concentrations (100–500 mg L^{-1}) [3, 4], most mining companies use sodium cyanide in excess. The problem is that leaching is not a selective process and cyanide can react with different metals existing in the ores (e.g., mercury, zinc, copper, iron, and nickel) forming various complexes. Consequently, effluents resulting from the leaching process may contain high amounts of residual cyanide [5].

The harmful environmental and toxicological characteristics of cyanide are well-documented [3]. Accordingly, many countries have developed legislation regarding cyanide concentration limits in industrial/mining originated effluents. For example: the US Environmental Protection Agency = 50–200 ppb, Germany and Switzerland = 0.01–0.5 mg L^{-1}, India = 0.2 mg L^{-1}, Mexico = 0.2 mg L^{-1}, and Colombia = 1 mg L^{-1} [6–8]. Several destructive and/or recovery processes have been developed to treat cyanide-containing solutions or slurries. Treatment methods include, but are not limited to: (i) physical (reverse osmosis [9], acidification, volatilization and reneutralization—AVR—[2], adsorption [10, 11], sulfurization, recycle and thickening—SART—[9, 12]) and (ii) chemical processes (alkaline chlorination [13], INCO process [2], hydrogen peroxide [14], Caro's acid [8], oxonization [15], biological treatment [16, 17], photochemical processes [18], and electrochemical methods [19]). Note that each technology presents limitations and drawbacks (e.g., effectiveness depending on cyanide concentration, the formation of toxic substances, high costs, generation of sludge, and additional byproducts).

Electrochemical (anodic) oxidation methods can transform cyanide into less harmful substances (e.g., cyanate, carbon dioxide, among others) and, consequently, the Chemical Oxygen Demand (COD) of the treated effluents can be reduced [20]. During electrolysis, heavy metals present in mining wastewater can be deposited on the cathode surface [19]. Thus, electrochemical processes can accomplish the destruction of cyanide and the reduction of heavy metal concentration simultaneously. Anodic oxidation may be direct, if cyanide oxidation occurs on anode surface, or indirect, if it involves ions that act as oxygen carriers generated in situ during the reaction. According to the literature [21], it has been proposed that the former is suitable for strong cyanide solutions (v.g., $[CN^-] > 1000$ ppm),

while the latter becomes relevant at high chloride concentrations (also known as electrochlorination process). Since mining wastewater can combine both conditions, it can be claimed that both direct charge transfer and oxygen carrier ions take part in the cyanide degradation process.

Different reaction pathways have been reported in the literature for the electrochemical oxidation (EO) of cyanide [21–23]. Among others, they include the following reactions:

Indirect oxidation mechanism :

$$\begin{aligned} &Cl^- + H_2O \rightarrow OCl^- + 2H^+ + 2e^- \text{ or} \\ &Cl_{2(gas)} + 2OH^- \rightarrow OCl^- + Cl^- + H_2O \\ &CN^- + OCl^- \rightarrow CNO^- + Cl^- \end{aligned} \quad (2)$$

Direct oxidation mechanism:

$$CN^- + 2OH^- \rightarrow CNO^- + H_2O + 2e^- \quad (3)$$

$$2CNO^- + 3OCl^- + H_2O \rightarrow N_2 + 2CO_2 + 3Cl^- + 2OH^- \quad (4)$$

$$CNO^- + 2OH^- \rightarrow CO_2 + \frac{1}{2}N_2 + H_2O + 3e^- \quad (5)$$

$$CNO^- + 2H_2O \rightarrow CO_3^{2-} + NH_4^+ \quad (6)$$

$$CNO^- + H^+ + 2H_2O \rightarrow HCO_3^- + NH_4^+ \quad (7)$$

Equation (4) represents cyanide mineralization. However, depending on the pH of the treated solution, other reactions (Eqs. 5–7) can also take place. Reaction (5) requires strong alkaline conditions (pH > 12). Conversely, the hydrolysis reaction presented in Eq. (7) occurs in weak alkaline solutions (7.0 < pH < 11.7). Finally, reaction (7) demands slightly acidic conditions [21].

Most of the previous studies on cyanide removal by EO were centered primarily around the effect of different anode materials on process efficiency. Valiūnienė et al. [19] applied platinum, titanium and stainless steel electrodes. The highest efficiency was obtained using the Pt electrode (the most expensive option). It allowed for a reduction of CN^- concentration from 0.1 M to 0.06 M during the first hour of electrolysis, while applying a current density of 200 A m^{-2}, with a current efficiency of ca. 80%. Felix-Navarro et al. [22] used reticulated vitreous carbon and graphite electrodes. The experiments were performed under different experimental conditions: supporting electrolytic media (NaOH, NaCl, $NaNO_3$, and Na_2SO_4), applied potentials (3.0, 4.0, 5.0, and 6.0 V) and volumetric flows of 130, 240, 480, 1058, and 1610 mL min^{-1} with recirculation. They reported the best conditions for cyanide degradation were observed when using NaCl (0.1 M) as supporting electrolyte, a cell potential of 5.0 V and a volumetric flow of 480 mL min^{-1}. Under these conditions, almost 100% cyanide degradation was achieved. Iordache et al. [24] investigated six types of electrodes (aluminum, titanium, nickel, copper, stainless steel (inox), and graphite) for the degradation of a synthetic solution of 0.1 mg CN^- mL^{-1}, using 1 mg NaCl mL^{-1} and applying current density of 0.03 A dm^{-2}. The highest efficiency was achieved using the graphite electrode. Indeed, in much of the research, graphite has proven to be an inexpensive and widely available material.

Actually, little work has been carried out [21] on the application of EO for the treatment of solutions containing high CN^- concentration (v. g., [CN^-] up to 1500 ppm, typical concentration in the case of gold mining effluents). Most of the reported information dealt with the EO of synthetic samples characterized with low CN^- concentration [19, 22]. Thus, high CN^- concentration represent engineering challenges to guarantee operators' safety and to satisfy new environmental legislations [8]. Hence, considering the available knowledge on cyanide depletion, a more detailed investigation on EO as an alternative for the treatment of wastewater containing high CN^- concentration is warranted. In this study, the effects of initial cyanide concentration, stirring velocity, pH, NaCl concentration, gap between electrodes, and current density on cyanide conversion were considered and were examined. As far as the authors are aware, there is no published analysis on the effect of different operational conditions and their interactions on cyanide and COD removal efficiencies, as well as on the energy consumption, performed using RSM based on the experimental design as well as on its assessment with industrial wastewater samples.

Thus, the objective of this research was to gain insight into the electrochemical oxidation of highly concentrated cyanide-containing effluent originating from a gold leaching industrial plant, located in the Caldas department (Colombia). The studied gold leaching effluent was monitored for 1 year. Its characteristics (v.g., initial cyanide concentration, $[CN^-]_0$, organic matter loading: Total Organic Carbon (TOC), COD, Biological Oxygen Demand (BOD_5), and biodegradability (BOD_5/COD ratio)) were measured. Significant changes in $[CN^-]_0$ (1000–2000 mg L^{-1}) were observed, depending on the ore being utilized at a given time. Thus, $[CN^-]_0$ was selected as a process variable. For optimization, a synthetic cyanide solution was used. The experiments were carried out in a laboratory-scale batch-jacketed electrolytic cell. Monopolar configuration of two electrodes, consisting of graphite (anode) and aluminum (cathode), was employed, operating in galvanostatic mode. This approach was selected with a look at the requirements of process scaling-up for the treatment of large volumes of the effluent. Response Surface Methodology (RSM), based on a Box–Behnken experimental Design (BBD),

Table 1 Summary of typical main physico-chemical characteristics of gold leaching effluent

Parameter	Permissible limit[a]	Wastewater sample	C–F supernatant	EO supernatant[c]
pH	6–9	11.5	11.1	9.54
Conductivity (μS cm^{-1})	n.r.	12,150 ± 1050	12,040 ± 1040	2580 ± 123
Chloride, Cl^-, (mg L^{-1})	250	3150 ± 270	3020 ± 102	2137 ± 27
Turbidity (NTU)	n.r.	146.5 ± 5.5	4.8 ± 0.2	4.0 ± 0.2
Total Cyanide (mg L^{-1})	1	1662.4 ± 10	1735 ± 34.6	0.13 ± 0,01
COD (mg O_2 L^{-1})	150	3734 ± 146	3795 ± 145	15 ± 5[b]
BOD_5 (mg O_2 L^{-1})	50	1.69 ± 0.25[b]	1.69 ± 0.25[b]	8.36 ± 0.25
Alkalinity (mg $CaCO_3$ L^{-1})	n.r.	4098.9 ± 48.8	3854.9 ± 45.9	2252.3 ± 32.5
TOC (mg C L^{-1})	n.r.	1206 ± 71	1434 ± 23	91.7 ± 5.3

The efficiency of coagulation–flocculation (C–F) pre-treatment and the permitted discharge limits are also included

n.r. not reported

[a]Emission limit values for industrial wastewater discharges according to Res 0631, 17/03/2015, issued by the Ministry of Environment and Sustainable Development, Colombia

[b]Quantification limit

[c]Results obtained after 180 min of EO treatment

was used to optimize the EO operational conditions. Three independent process variables were considered: initial cyanide concentration ($[CN^-]_0 = 1000–2000$ mg L^{-1}), current density ($J = 7–107$ mA cm^{-2}), and stirring velocity ($\eta = 250–750$ rpm). The cyanide conversion $\left(X_{CN^-}\right)$, COD removal percentage ($\%R_{COD}$), and specific Energy Consumption per unit mass of removed cyanide (EC) were analyzed as response variables. Moreover, a multi-objective optimization including both maximization of cyanide conversion and minimization of energy consumption was accomplished. The changes in cyanide concentration, COD, TOC, and the evolution of some reactive intermediates were monitored with kinetic analysis. Next, gold leaching effluent was treated. Initially, the operational conditions of its pre-treatment by coagulation–flocculation (C–F) were determined and the obtained supernatant was characterized. Then, it was treated by the EO process at experimental conditions optimized using synthetic cyanide solution. The predictive capacity of fitted models was verified against C–F–EO experimental data obtained for gold leaching effluent. Finally, in order to determine the minimum time required to accomplish the permissible Colombian discharge limits, the variation of free and total cyanide as well as COD with time was followed.

2 Materials and methods

2.1 Wastewater samples

The cyanide-containing wastewater samples were taken from an equalization tank of a gold leaching industrial plant, located in the Caldas department (Colombia). In order to determine its representative characteristics, the sampling was performed bimonthly for 1 year. For sampling, preservation, storage and transportation, the EPA wastewater-monitoring guide and Standard Methods were followed [2, 25]. Typical main characteristics of the wastewater are presented in Table 1. Notice that the high conductivity of studied effluent is a result of the presence of different metals and anions in the ore and consequently in the effluent. High concentration of cyanide is directly related to the characteristics of the applied leaching process, which, in turn, implies a high COD value, significantly exceeding legislation limits. The presence of cyanide imposes restrictions to the pH of the treatment process. Thus, the treated solutions must be strongly alkaline in order to prevent cyanide volatilization. Additionally, the initial BOD_5/COD ratio, equaled to 4.52×10^{-5} (< 0.4), implies that the wastewater is non-biodegradable [26]. Moreover, oxygen consumption was not detectable during BOD_5 measurements, indicating that the wastewater conditions are not suitable for microorganism growth. Thus, for this parameter, the quantification limit was reported in Table 1.

2.2 Reagents

All reagents were used as received, without any further purification. Sodium hydroxide (NaOH, Carlo Erba, 97 wt%) and potassium cyanide (KCN, PanReac, 97 wt%) were used to prepare the synthetic cyanide solutions required to perform BBD-RSM experiments. Silver nitrate ($AgNO_3$, PanReac, 99.8 wt%) and p-dimethylaminobenzalrhodanine ($C_{12}H_{12}N_2OS_2$, Across Organic, 99 wt%) were used to measure the concentration of cyanide by titration in the range of 1–10 mg L^{-1}. Barbituric acid (Alfa Aesar, 99 wt%), chloramine-T (Carloerba, analytical grade), and

pyridine (Mallinckrodt, 99 wt%) were used to measure cyanide concentration by a colorimetric method in the range of 0.02–0.2 mg L^{-1}. The corresponding aqueous solutions were prepared using ultra-pure water (Milli-Q system, conductivity < 1 MμS cm^{-1}). Sodium chloride (NaCl, Carlo Erba, 99 wt%) was used in the electrochemical process as support electrolyte. The solution pH was measured using a pH-meter Accumet® AB15, equipped with an BOECO-BA-25 electrode, and adjusted with 4 M nitric acid (HNO_3, Merck, 65 wt%). Ferric chloride ($FeCl_3$) was used for the coagulation–flocculation pre-treatment. Sulfuric acid (Merck 95–97 p.a.) was used to measure ammonia and cyanate before hydrolysis.

2.3 Analytical methods

Standard methods were followed for the quantitative analysis of the effluent: turbidity (2130 B, NANOCOLOR® UV/VIS spectrophotometer), conductivity (2510-B, conductivimeter LAB-960 Analytics), alkalinity (titrimetric method (2320 B) with standard 0.1 N sulfuric acid), and pH (pH-meter LAB-850-Analytics).

The titrimetric (4500-CN^- D) and colorimetric (4500-CN^- E) Standard Methods were implemented to measure and track the changes in cyanide concentration [25]. In the titrimetric method, the alkaline distillate from the preliminary treatment (4500-CN^- C), was titrated with standard 0.018 M $AgNO_3$ to form soluble cyanide complex, $Ag(CN)_2^-$. As soon as all CN^- were complexed and a small excess of Ag^+ was added, the excess of Ag^+ was detected by the silver-sensitive indicator, p-dimethylaminobenzalrhodanine, which immediately changed the solution color from yellow to salmon pink. If the titration resulted in a CN^- concentration below 1 mg L^{-1}, another portion of solution was examined colorimetrically. In the colorimetric method, the alkaline distillate, from preliminary treatment (4500-CN^- C), was converted to CNCl by reaction with chloramine-T, at pH < 8 without hydrolyzing to CNO^-. Upon completion, CNCl resulted in a purple color after the addition of pyridine-barbituric acid reagent. The absorbance of the solution was measured at 578 nm wavelength, using a NANOCOLOR® UV/VIS spectrophotometer. In order to measure total cyanide levels, samples were pre-treated by distillation and free cyanide was measured directly without any additional treatment.

The titrimetric (4500-NH_3 C) Standard Method was used to determine ammonia and cyanate concentrations. At first, ammonia-containing solutions were pre-treated by distillation using a boric acid solution as an absorbent for the distillate (4500-NH_3 B). Then, the distillated solutions were titrated with standard 0.02 N sulfuric acid until the indicator color turned into pale lavender. Bearing in mind that the cyanate hydrolyzes to ammonia if it is heated at low pH, the samples were acidified (pH 2.0–2.5) and heated up to 90 to 95 °C. The ammonia concentration was measured by the titrimetric Standard Method (4500-NH_3 C).

The COD analyses were performed by closed reflux method (NANOCOLOR® thermoreactor Vario C2) with colorimetric determination (NANOCOLOR® UV/VIS spectrophotometer), at 620 nm (100–1500 mg O_2 L^{-1}) or 436 nm (15–160 mg O_2 L^{-1}), Standard Method 5220D.

TOC-L SHIMADZU equipped with a non-dispersive infrared detector was used to quantify the contents of total carbon (TC), inorganic carbon (IC) and total organic carbon (TOC). The analysis was carried out by catalytic combustion of the sample (at 680 °C), in the quantification range of 0.03–1000 mg C L^{-1}.

The 5 days BOD tests (BOD_5) were performed following the respirometric Standard Method (5210 B).

2.4 Experimental setup

EO experiments were performed in a 150 mL all-glass batch-jacketed electrolytic cell, loaded at 80% capacity. The solution was stirred mechanically using a stirring plate (Isotemp® 1120049SH) and a magnetic stirrer (2.5 cm). On the top of the cell, a PT-100 sensor (± 0.01 °C) was placed to measure solution temperature. All experiments were performed at 20 °C (± 0.05 °C), regulated using a thermostated water bath (F-12, Julabo-Germany) connected to the reactor jacket. The electrolytic cell consisted of two vertical, rectangular, plate electrodes: a graphite anode (EC-12 grade), with a total area of 6.65 cm^2 (effective area of 2.25 cm^2), and an aluminum cathode (Al-1100, pure aluminum content > 99%), with a total area of 5.36 cm^2 (effective area of 2.25 cm^2). They were disposed vertically into the cell and connected in a monopolar arrangement to a DC power source (BK-Precision, 0–30 V, 0–5 A, Yorba Linda, California), operating in galvanostatic mode. The gap between electrodes was setup at 5 mm (see Supplementary Material). Before each run, the aluminum electrode was rubbed with sand paper and dipped in a concentrated solution of HCl (35 v/v %) for ca. 5 min to remove impurities from the surface. Then, it was rinsed with distilled water. The graphite electrode was dipped into deionized water for 5 min. Both electrodes were dried in an oven (Thermo Scientific™ Heratherm™) at 105 °C. Wastewaters used in the experiments contained 0.15 M of NaCl as a support electrolyte. For each experiment, sample pH was adjusted using NaOH to the value of 11.1 (which corresponds to the value of C–F supernatant pH) and controlled using a pH-meter (Fisher Scientific™ accumet™ AB15 Basic).

The efficiency of EO process was evaluated with cyanide conversion $\left(X_{CN^-}\right)$, COD removal percentage ($\%R_{COD}$), and specific Energy Consumption per unit mass of removed cyanide (EC, kWh kg^{-1}), Eqs. (8–10), as follows:

$$X_{CN^-} = \frac{[CN^-]_0 - [CN^-]}{[CN^-]_0} \quad (8)$$

$$\%R_{COD} = \frac{COD_0 - COD}{COD_0} \times 100 \quad (9)$$

$$EC = \frac{1000 \cdot VI \cdot t}{\Delta[CN^-] \cdot V_R} \quad (10)$$

where V is voltage (V), I corresponds to current intensity (A), t is the reaction time (h), V_R is the volume of the reacting mixture (L), and $\Delta[CN^-]$ equals to $([CN^-]_0 - [CN^-]_t)$ (mg L^{-1}).

2.5 Coagulation–flocculation pre-treatment

Before EO, a gold leaching effluent sample was pre-treated by a coagulation–flocculation (C–F) process. Its operational conditions were determined following the jar test standard procedure (ASTM D2035:2008). This process consisted of three steps: (i) a period of fast mixing (at 150 rpm) of the wastewater solution with $FeCl_3$ for 2 min; (ii) a period of slow mixing (at 20 rpm) for 20 min to induce the flocs' formation; and (iii) 15 min of sedimentation without agitation. This sequence allowed for the determination of the optimal coagulant dose using as a standard the most significant turbidity removal. After completing the C–F process, the obtained supernatant was characterized and treated by EO process.

2.6 Selection of EO independent variables and their levels. Preliminary experiments

EO independent variables and their levels for an experimental design were selected according to the cyanide-containing effluent characteristics and results of preliminary experiments. The effects of initial cyanide concentration, stirring velocity, pH, NaCl concentration, gap between electrodes, and current density on cyanide conversion were considered and were examined (for details see Supplementary Material).

Table 2 Process variables levels for experimental design

Symbol	Factors	Unit	Coded levels		
			−1	0	1
A	Initial cyanide concentration ($[CN^-]_0$)	mg L^{-1}	1000	1500	2000
B	Current density (J)	mA cm^{-2}	7	57	107
C	Stirring velocity (η)	rpm	250	500	750

2.7 Experimental design and statistical analysis

Response Surface Methodology (RSM), based on a Box–Behnken experimental Design (BBD), was used to optimize the EO operational conditions. RSM involves of a group of mathematical and statistical techniques based on the fitting of empirical models to the experimental data obtained according to the selected matrix. Next, linear or square polynomial functions are used to describe the performance of the studied system and to examine the experimental conditions until their optimization [27]. Its application as an optimization tool involves the following steps: (i) the choice of independent variables with major effects on the studied system (factors) and the definition of their experimental range; (ii) the selection of dependent variables (responses); (iii) the selection of the experimental design and its experimental running; (iv) the mathematical and statistical treatment of the obtained experimental data (fitting to a polynomial function); (v) the evaluation of the fitted model; (vi) the optimization; (vii) model validation. Thus, three independent process variables (factors) were selected: initial cyanide concentration ($[CN^-]_0$ = 1000–2000 mg L^{-1}), current density (J = 7–107 mA cm^{-2}) and stirring velocity (η = 250–750 rpm) (for details see Supplementary Material). The cyanide conversion (X_{CN^-}), COD removal percentage ($\%R_{COD}$), and specific Energy Consumption per unit mass of removed cyanide (EC) were analyzed as response variables. Next, the experimental design was implemented to determine the effect of different operating factors (initial cyanide concentration, current density, and stirring velocity) and their interactions on EO efficiency (v.g., X_{CN^-}, EC and $\%R_{COD}$). Three different levels (values) were chosen for each of the three listed variables. In this part of the study, synthetic samples were used according to the characterization of C–F supernatant. The independent variables and their levels are summarized in Table 2.

A multifactorial, three-central points, Box–Behnken experimental Design (BBD) was applied. BBD belongs to a class of rotatable or nearly rotatable second-order designs based on three-level incomplete factorial designs [28]. These designs are considered as less expensive than their corresponding 3^k designs. The number of experiments (N) required for the development of BBD is defined as $N = 2k\ (k-1) + C_0$, (where k is number of factors and C_0 is the number of central points). For comparison, the number of experiments for a central composite design (CCD) is $N = 2^k + 2k + C_0$. Concerning the efficiency, defined as the number of coefficients in the estimated model divided by the number of experiments [28], of the following three factors designs: CCD, Doehlert design (DD), BBD, and three-level full factorial design, BBD and DD result slightly more efficient than the CCD and much more efficient than the three-level full factorial designs. Another characteristic of BBD is

Table 3 The experimental and predicted results of X_{CN^-}, $\%R_{COD}$ and EC (and their standard deviations) for the EO processes according to the BBD

Test	$[CN^-]_0$ (mg L^{-1})	J (mA cm^{-2})	η (rpm)	X_{CN^-}	±	EC (kWh kg^{-1})	±	$\%R_{COD}$	±
1	1500	57	500	0.33	0.00	17.73	1.75	23.21	3.06
2	2000	107	500	0.53	0.01	35.22	2.47	36.70	7.35
3	2000	7	500	0.15	0.02	2.29	0.04	7.57	7.46
4	2000	57	250	0.26	0.00	19.37	0.54	17.81	2.70
5	1500	107	250	0.59	0.04	43.98	2.63	51.32	7.18
6	2000	57	750	0.27	0.03	15.07	2.42	9.86	4.43
7	1000	57	250	0.36	0.01	25.89	0.20	12.12	0.71
8	1500	57	500	0.34	0.01	17.48	1.07	30.55	1.46
9	1500	7	250	0.12	0.00	3.29	0.27	0.38	0.53
10	1500	57	500	0.35	0.08	17.38	0.64	24.25	13.03
11	1500	7	750	0.11	0.00	3.07	0.29	8.65	3.72
12	1500	107	750	0.60	0.01	37.87	2.47	45.11	2.92
13	1000	7	500	0.18	0.01	3.19	0.00	16.41	0.36
14	1000	107	500	0.66	0.00	44.84	8.26	46.59	3.04
15	1000	57	750	0.43	0.05	18.39	1.32	40.03	3.39

Reaction time = 40 min

lack of combinations at which all factors are simultaneously at their highest or at their lowest levels, letting to avoid the running of experiments under extreme conditions. In this way, BBD will contain regions of poor prediction quality (like missing corners). However, this property can be useful if the researcher should avoid combined factor extremes. It also prevents a potential loss of data in these cases. Considering all these characteristics, BBD was chosen and applied in this study.

Thus, 15 experiments, each replicated twice, were randomly performed to avoid any systematic error. They were programmed using Statgraphics Centurion XVIII® (30-day trial version is available at http://www.statgraphics.net). The total electrolysis time was fixed in 40 min. Multi-objective optimization analysis was carried out to establish the most effective electrolysis conditions.

For the RSM, the experimental results were fitted to a second-order multivariable polynomial, as presented in Eq. (11):

$$Y = \beta_0 + \sum_{i=1}^{n} \beta_i x_i + \sum_{i=1}^{n} \beta_{ii} x_i^2 + \sum_{i=1}^{n-1} \sum_{j=i+1}^{n} \beta_{ij} x_i x_j \quad (11)$$

where Y is the response variable (v.g., X_{CN^-}, o EC, o $\%R_{COD}$); β_0, β_i, β_{ii}, and β_{ij} are the regression coefficients. β_0 is the intercept, β_i are the main effects, β_{ii} are the quadratic effects and interactions; x_i and x_j are the independent variables ($[CN^-]_0$, J and η).

The quality of this model and its prediction capacity were judged from the correlation coefficient, R^2, and standard deviation value (σ). The main effects and the interaction effects of different factors on the response variables was followed by analysis of variance (ANOVA). The ANOVA consists of classifying and cross-classifying statistical results. Fisher F test, defined as the ratio of respective mean-square effect and mean-square error, was used to evaluate the presence of a significant difference from control response and to calculate standard errors. The p values were used to identify experimental parameters that have a statistically significant influence on particular response. If p value is lower than 0.05, it is statistically significant with the 95% confidence level [29]. Additionally, statistical analysis was completed with a Pareto diagram and a correlation coefficient examination.

In order to optimize EO (v.g., to achieve the highest cyanide removal with the lowest energy consumption), a multi-objective optimization analysis was carried out using the *fmincon* function available in MatLab® software. It included the minimization of the following objective function:

$$F_{obj} = \min \left[\sum_{i=1}^{M} w_i f_i(x) \right] \quad (12)$$

where w_i is the weight factor and $f_i(x)$ corresponds to the quadratic polynomial fitted for the cyanide removal and for the specific energy consumption.

Model validation was performed experimentally at optimized conditions (Sect. 3.2.3) as well as at some arbitrary chosen conditions (for details see Supplementary Material).

2.8 Kinetic analysis and tests with industrial gold leaching effluent

A kinetic study was carried out at the optimized conditions of EO. Kinetic power law expressions were fitted for cyanide (CN^-), cyanate (CNO^-), COD, and TOC data. They allowed for the determination of time required to meet permissible Colombian discharge limits. Simulation results were

compared with the experimental data obtained using the C–F–EO process performed with the gold leaching effluent.

3 Results and discussion

3.1 Wastewater pre-treatment by coagulation–flocculation

In order to establish the optimal C–F conditions, the jar test was performed using different concentrations of $FeCl_3$ (in the range of 20–250 mg $FeCl_3$ L^{-1}). The most significant turbidity removal, equivalent to ca. 97%, was observed using 100 mg L^{-1} of $FeCl_3$ dosage. It was chosen as the working coagulant concentration for C–F. In these conditions, the C–F supernatant was characterized. Its physico-chemical features were compared with those corresponding to the gold leaching effluent (Table 1). Note that the C–F process was unable to reduce/remove organic loading from the sample. Its biodegradability ratio BOD_5/COD also remained almost unchanged (4.45×10^{-4}), rendering any biological treatment inadequate for this type of residual waste. Thus, before its final disposal, additional treatment was required. Also, notice that after the C–F, the effluent's pH remained unchanged. Cyanide concentration increased ca. 5% probably due to the destruction of cyanide–metal complexes during the C–F process.

3.2 The electro-oxidation process

3.2.1 Box–Behnken experimental design and polynomial regression

Experimental design (experimental conditions) together with the obtained average results of X_{CN^-}, $\%R_{COD}$ and EC (and their standard deviations) are given in Table 3.

The highest percentage of COD removal was ca. 51%, achieved at the following experimental conditions: $[CN^-]_0 = 1500$ mg L^{-1}, $J = 107$ mA cm^{-2}, and $\eta = 250$ rpm. These conditions also allowed for a ca. 60% of cyanide conversion. Notice that 107 mA cm^{-2} corresponds the highest values of conversion. In these two cases, the EC equaled to 43.98 kWh kg^{-1}.

Multiple polynomial regression was carried out to fit experimental data to the second-order polynomial models (Eq. 11). The obtained regression coefficients are included in Eqs. (13–15). The goodness of fit was estimated through the correlation coefficient (R^2) and the adjusted correlation coefficient (R^2_{adj}). Their values indicated that fitted polynomial models describe ca. 99% of the variability observed in the X_{CN^-} and EC data and 95% for R_{COD}. The R^2_{adj} is a more rigorous parameter to determine the quality of the models. Likewise, the obtained model can describe ca. 87% of the R_{COD} variability observed in the experimental data. The quality of the model was also evaluated basing on standard deviation value (σ); the lower value of standard deviation, more accurate the response predicted by the model. Notice that the following values of standard deviation 0.265, 0.891, 5.900 were obtained for the models described by the Eqs. (13–15), respectively:

$$X_{CN^-} = 0.0938 - 7.8 \times 10^{-5}A + 0.0044B + 4.772 \times 10^{-4}C + 3 \times 10^{-8}A^2 - 1 \times 10^{-6}AB - 1.2 \times 10^{-7}AC + 1.3 \times 10^{-5}B^2 + 4 \times 10^{-7}BC - 2.8 \times 10^{-7}C^2 \quad (13)$$

$$R^2 = 99.22 \quad R^2_{adj} = 97.82$$

$$EC = 18.6525 - 0.0122A + 0.4229B - 0.345C + 2.965 \times 10^{-6}A^2 - 8.72 \times 10^{-5}AB + 6.4 \times 10^{-6}AC + 1.2455 \times 10^{-3}B^2 - 1.178 \times 10^{-4}BC + 2.254 \times 10^{-5}C^2 \quad (14)$$

$$R^2 = 99.87 \quad R^2_{adj} = 99.63$$

$$\%R_{COD} = -80.6341 + 0.0592A + 0.3626B + 0.1871C - 1.1192 \times 10^{-5}A^2 - 1.05 \times 10^{-5}AB - 7.172 \times 10^{-5}AC + 1.4448 \times 10^{-3}B^2 - 2.896 \times 10^{-4}BC - 5.2007 \times 10^{-5}C^2 \quad (15)$$

$$R^2 = 95.23 \quad R^2_{adj} = 86.65$$

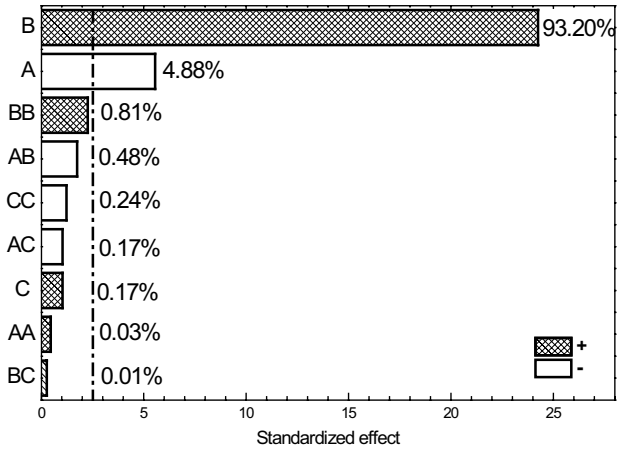

(a)

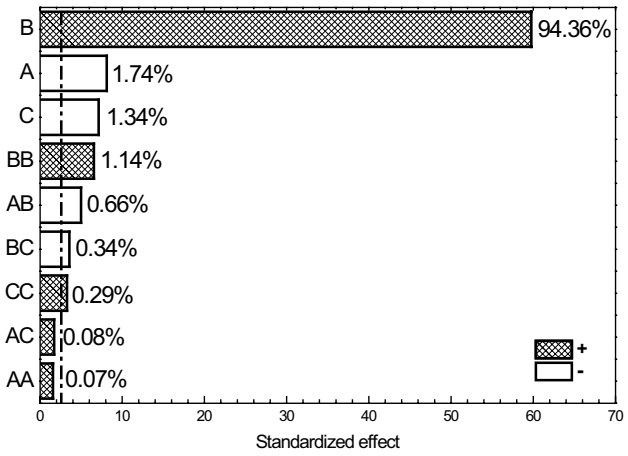

(b)

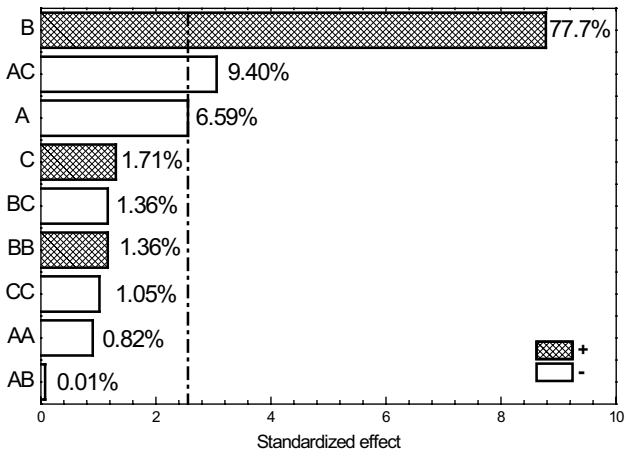

(c)

Fig. 1 Pareto diagrams for: X_{CN^-} (**a**), EC (**b**) and $\%R_{COD}$ (**c**)

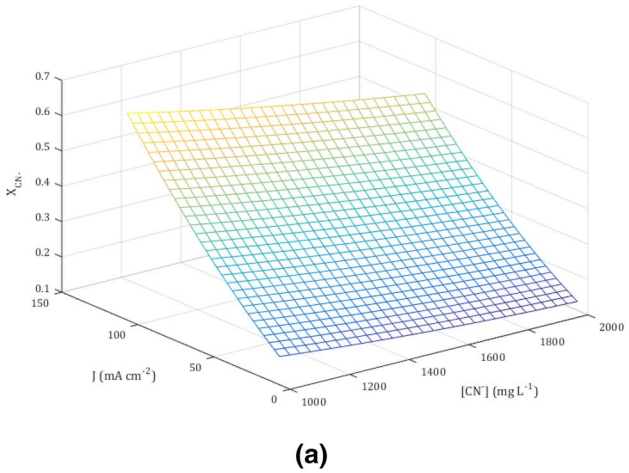

(a)

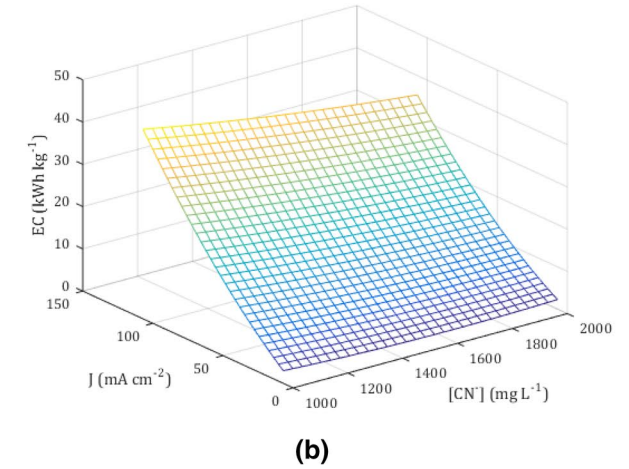

(b)

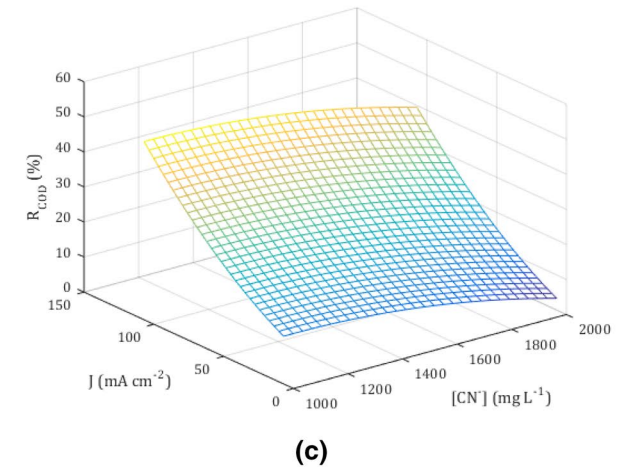

(c)

Fig. 2 Three-dimensional surface response plots obtained for the interactive effect of J and [CN^-] on: X_{CN^-} (**a**), EC (**b**) and R_{COD} ($\eta = 500$ rpm) (**c**)

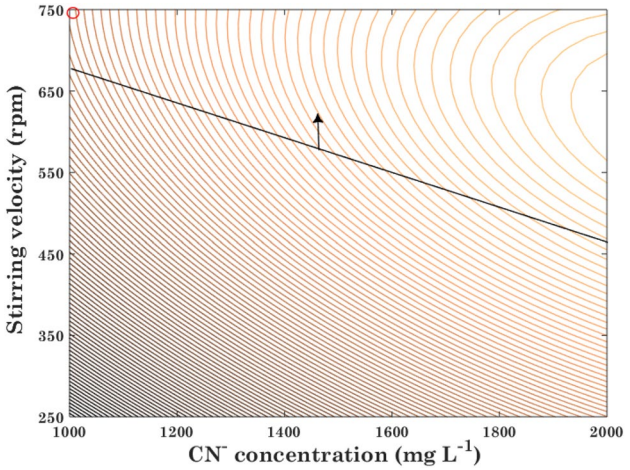

Fig. 3 Contour plot of results obtained using multi-objective optimization

3.2.2 Statistical analysis

The statistical analysis was based on Pareto diagrams, response surface plots and analysis of variance (ANOVA). The Pareto diagram illustrates the statistical significance of each factor and its interactions. It represents graphically the standardized effects from the highest to the lowest in magnitude as a series of bars whose heights (b_i) reflect the influence of each factor. The bars are organized in descending order of heights from left to right. Therefore, the factors characterized by the tallest bars are relatively more significant. The bar sign indicates if an increase in the level of the factor presents a positive (+) or negative (−) effect on the response variable. Figure 1 presents Pareto diagrams for X_{CN^-}, EC and $\%R_{COD}$ using EO process, including the percentage effect of each factor (P_i) according to Eq. (16) [30]:

$$P_i = \left(\frac{b_i^2}{\sum b_i^2} \right) \times 100 \tag{16}$$

Statistically important factors, with a confidence of 95% (using t Student distribution), correspond to all bars with values crossing the internal vertical line. They coincide with values established with the variance analysis (ANOVA). According to ANOVA results (Tables SM2–SM4, Supplementary Material), one can see that all terms in the regression models are not equally important. Notice that both $[CN^-]_0$ and J presents p value < 0.05, which implies that they have a truthful effect on the three response variables (X_{CN^-}, EC and $\%R_{COD}$), with the confidence interval of 95%. Moreover, as expected, the EC strongly depends on η and on some interactions between the following variables: $[CN^-]_0 - J$, $J - J$, $J - \eta$, and $\eta - \eta$. It can also be noticed that the interaction $[CN^-]_0 - \eta$ has statistical significance on $\%R_{COD}$.

For each of three response variables, the current density presents statistically the most significant effect. Its positive sign indicates that the highest degradation efficiency was obtained at the highest level of this factor. The initial cyanide concentration also shows statistical significance. However, in all cases, cyanide conversion is inversely proportional to cyanide concentration. Notice that in the studied range, the stirring velocity does not affect neither the X_{CN^-} nor the efficiency of COD removal. This phenomenon can occur due to the oxidation of cyanide to cyanate (Eq. 3), near to the

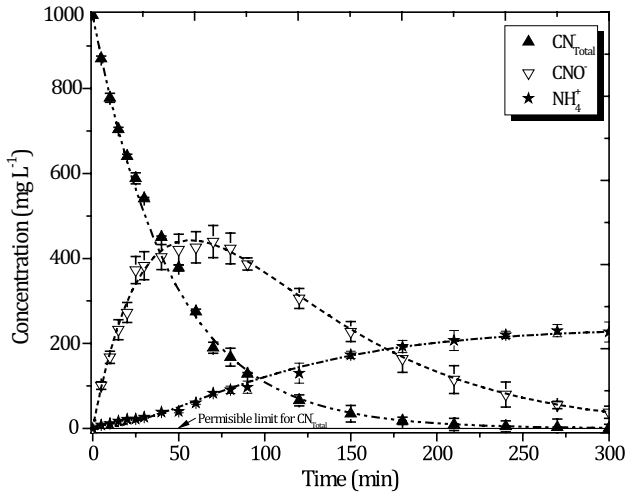

Fig. 4 The variation of cyanide (CN^-), cyanate (CNO^-) and ammonium (NH_4^+) concentrations vs. time. EO operational conditions: $[CN^-]_0 = 1000$ mg L^{-1}, $J = 100$ mA cm^{-2}, $\eta = 750$ rpm, [NaCl] = 0.15 M and pH 11.1

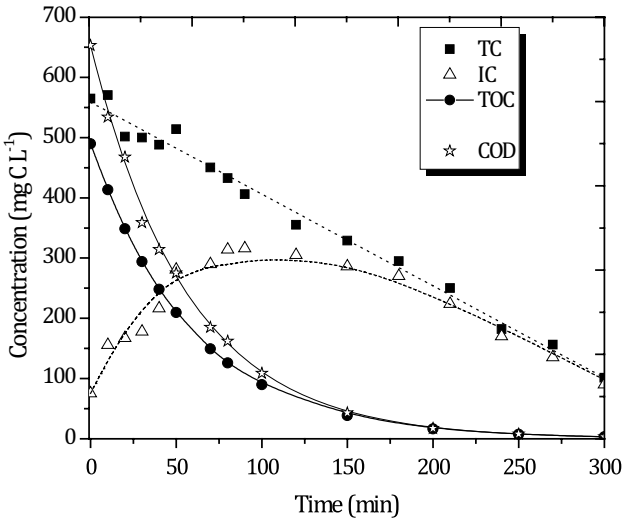

Fig. 5 The variation of TC, IC and TOC concentrations vs. time. EO operational conditions: $[CN^-]_0 = 1000$ mg L^{-1}, $J = 100$ mA cm^{-2}, $\eta = 750$ rpm, [NaCl] = 0.15 M, and pH 11.1

electrode surface, and its subsequent migration to the bulk where it is mineralized (Eq. 4).

In order to determine the integrated effect of both J and $[CN^-]_0$ on the response variables, three-dimensional Box–Behnken response surface plots, at a constant η value of 500 rpm (halfway in the studied range of this factor) were used (Fig. 2). Notice that X_{CN^-}, EC and $\%R_{COD}$ increase with an increase in J, as it can be expected in any electrochemical process. Moreover, their highest value correspond to the lowest value of cyanide concentration. These results agree with the literature findings [21]. Visual inspection of the obtained surfaces does not let to define the optimal conditions for the simultaneous maximization of cyanide conversion and minimization of EC. Thus, a multi-objective optimization analysis was undertaken.

3.2.3 Multi-objective optimization analysis

Considering the results of statistical analysis and the interest in simultaneous maximization of the X_{CN^-} and minimization of the EC, a multi-objective optimization was carried out. Thus, Eqs. (12–15) were simultaneously solved using the *fmincon* function available in MatLab® software. The following constrains were included in the optimization analysis: (i) the removal of total cyanide from the effluent must meet Colombian regulations (i.e., $[CN^-] < 1$ mg L^{-1}) and (ii) the weight factor (w) for the EC must be lower than the maximum value measured experimentally (i.e., $w_{EC} \leq 44.84$, see Table 3). The obtained results are presented as a contour plot in Fig. 3. The optimization constrictions and the optimal operating conditions are identified as a black line and a red circle, respectively, and they correspond to: $[CN^-]_0 = 1000$ mg L^{-1}, $J = 100$ mA cm^{-2}, and $\eta = 750$ rpm. At these conditions, the experimental verification of EO efficiencies, predicted by the Eqs. (13–15), was performed. The following results were obtained: $X_{CN^-} = 0.68 \pm 0.01$, $\%R_{COD} = 52.6 \pm 8.99$, and EC $= 41.86 \pm 0.4$ kWh kg^{-1} (measured values) vs. $X_{CN^-} = 0.65$, $\%R_{COD} = 52.63$, and EC $= 38.2$ kWh kg^{-1} (predicted values), confirming the high predictive capacity of the model. The model was also successfully tested under arbitrary experimental conditions (for details see page 6 in Supplementary Material). However, 40 min of electrolysis did not result in the permissible limit of cyanide content (< 1 mg L^{-1} or $X_{CN^-} = 0.999$), required by Colombian legislation. Thus, at the optimized operational conditions, the evolution of EO with time was performed.

3.2.4 Kinetic study

Figure 4 presents the variation of total cyanide (CN^-), cyanate (CNO^-) and ammonium (NH_4^+) concentrations with time.

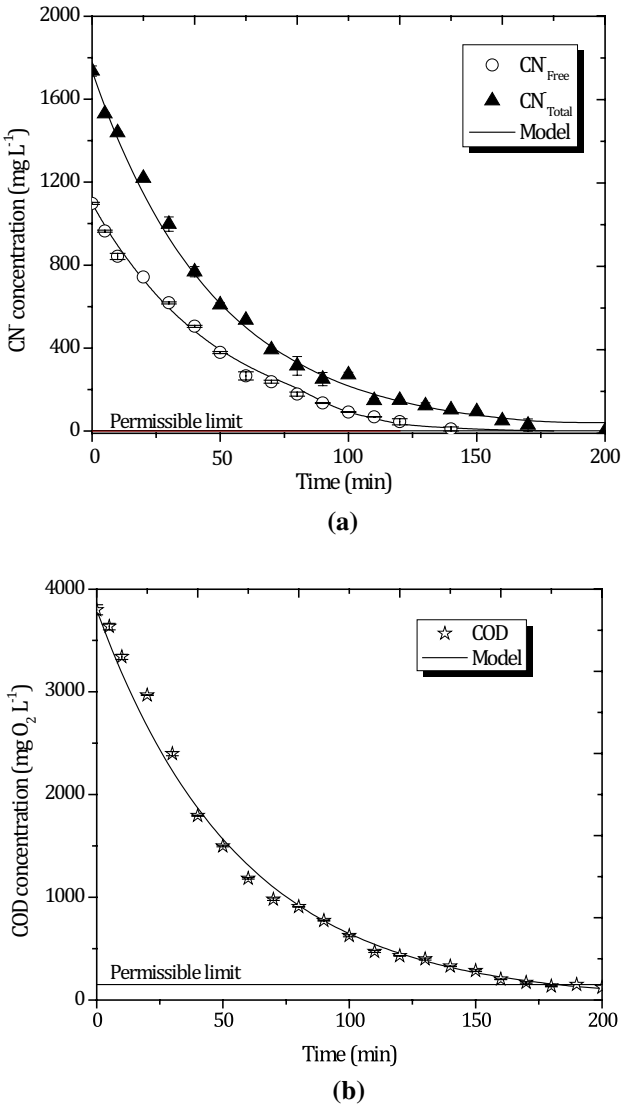

Fig. 6 The variation of free and total cyanide (**a**) and COD (**b**) concentrations vs. time for the gold leaching effluent treated by EO (sample after C–F treatment, see Table 1). Comparison between experimental data, model results and permissible discharge limits

According to the path for cyanide mineralization, cyanate formation and its subsequent decomposition is a consequence of a series of reactions, outlined in Eqs. (2–7). One can see (Fig. 4) that the total cyanide concentration decreases with time, reaching X_{CN^-} of 0.999 (= 1 mg L^{-1}) after 210 min of reaction. The cyanate concentration increases gradually with the reaction time reaching a maximum at ca. 55 min of electrolysis. Next, its concentration decreases monotonically. The ammonium concentration increases progressively during the treatment, reaching a value of 228 mg L^{-1} after 300 min. Notice that cyanate ions are significantly less toxic than cyanide, and

ammonium is a complete mineralization product of cyanide although it can also be toxic.

Carbon evolution along the EO process was also analyzed. Depending on the pH values, carbon can be present in cyanide, cyanate, carbon dioxide, and/or as carbonate or bicarbonate species. As EO takes place at an initial pH of ca. 11, and slightly decreases during the reaction without reaching values below 10, carbon existing in the cyanide and cyanate ions can be oxidized to form carbonate and bicarbonate species. The variation of total carbon (TC), inorganic carbon (IC) and TOC concentration vs. time is presented in Fig. 5. The TOC concentration decreases gradually reaching total removal after ca. 250 min of EO. The IC concentration increases gradually with reaction time reaching a maximum at ca. 100 min of electrolysis. Next, its concentration decreases monotonically. This behavior implies that carbon was effectively transformed from its reduced to its oxidized form (v.g., CO_2, CO_3^{2-}, HCO_3^-). The COD concentration, similarly to TOC, decreases continuously during the EO process and yielded a total removal after ca. 250 min.

Data fitting was performed for kinetic parameters adjustment. At first, molar balance equation was applied to the batch reactor. To solve the reactor model, an expression for the reaction rate was required. Since electrochemically generated compounds are very reactive, it is natural to consider a first-order kinetic law expression, such as follows [31]:

$$r_i = k_i C_i \tag{17}$$

Molar balances were derived as a function of the reaction rates of the compound in the solution (CN^- and CNO^-) obtaining:

$$\frac{dC_{CN^-}}{dt} = -k_{CN} C_{CN^-} \tag{18}$$

$$\frac{dC_{CNO^-}}{dt} = k_{CN} C_{CN^-} - k_{CNO} C_{CNO^-} \tag{19}$$

Moreover, the COD and TOC data were also adjusted to the first-order kinetics expressions as follows:

$$\frac{dC_{COD}}{dt} = -k_{COD} C_{COD} \tag{20}$$

$$\frac{dC_{TOC}}{dt} = -k_{TOC} C_{TOC} \tag{21}$$

Parameters with the highest R^2 were selected. Thus, the following kinetic constants were obtained: $k_{CN^-} = (2.19 \pm 0.097) \times 10^{-2}$ min^{-1} ($R^2 = 0.9944$), $k_{CNO^-} = (1.38 \pm 0.17) \times 10^{-2}$ min^{-1} ($R^2 = 0.9633$), $k_{COD} = (1.77 \pm 0.099) \times 10^{-2}$ min^{-1} ($R^2 = 0.9838$) and $k_{TOC} = (1.68 \pm 0.145) \times 10^{-2}$ min^{-1} ($R^2 = 0.9852$). The predicted values for all models were included as lines in Figs. 4 and 5.

3.2.5 EO as an alternative for mineralization of cyanide originating from gold leaching effluent

Finally, the EO of cyanide originating from gold leaching effluent was carried out. For this purpose, the C–F supernatant was used (Table 1). Thus, the obtained kinetic expressions were used to predict the electrolysis time required to reach the legislated permissible limits for total cyanide content (Table 1). The evolution of free and total cyanide concentrations (Fig. 6a) as well as COD (Fig. 6b) was monitored as a function of time. One can see that the fitted models effectively describe the experimental data. Thus, after ca. 180 min of EO, under the following operating conditions: ($[CN^-]_0 = 1735$ mg L^{-1}, $J = 100$ mA cm^{-2}, and $\eta = 750$ rpm) (Table 1), legislated permissible limits for both total cyanide and COD were achieved. The required EC corresponded to 71.33 kWh kg^{-1}. Moreover, the BOD_5/COD biodegradability ratio changed from 4.52×10^{-4} to 0.5573, representing a very significant increase in the biodegradability of the studied effluent (BOD_5/COD > 0.4 classifies an effluent as biodegradable). Additional information regarding the reaction evolution during the EO can be obtained analyzing the average oxidation state (AOS) of the treated sample. It can be calculated as follows [32]:

$$\mathrm{AOS} = 4 - 1.5\frac{\mathrm{COD}}{\mathrm{TOC}} \tag{22}$$

where COD and TOC are expressed in mg O_2 L^{-1} and mg C L^{-1}, respectively. The AOS can take values between −4 (for the most reduced state of carbon, CH_4) and +4 (for the most oxidized state of carbon, CO_2). An AOS value of −0.64 was estimated for the gold leaching effluent. However, at the end of C-F-EO process, an AOS reached the value of 3.75, indicating significant carbon oxidation (reaching a state similar to that of CO_2) and an effective mineralization of the studied effluent. This characteristic usually improves wastewater biodegradability.

4 Conclusions

An electrochemical oxidation was applied as an alternative for the treatment of cyanide originating from gold leaching effluent. This effluent presented both high conductivity (12,150 µS cm^{-1}) and high cyanide concentration (1662 mg L^{-1}) and it could not be treated by biological methods (BOD_5/COD = 4.52×10^{-4}). Drawing from the experimental design, response surface methodology, and multi-objective optimization analysis, the following optimal

EO operational conditions were established: initial cyanide concentration = 1000 mg L^{-1}, current density = 100 mA cm^{-2}, and stirring velocity = 750 rpm. They were verified experimentally. The experimental data (X_{CN^-}, $\%R_{COD}$, and EC) were fitted to second-order polynomial models with adjusted correlation coefficients (R^2_{adj}) of ca. 98, 99, and 87%, respectively. The kinetic analysis, performed at optimal EO operational conditions, allowed determination of time (180 min) required to meet Colombian permissible discharge limits for COD and total cyanide content. The predictive capacity of kinetic expressions was verified against C–F–EO experimental data obtained for cyanide-containing effluent originating from gold leaching process. Total cyanide removal and 96% of COD reduction was reached, requiring EC of 71.33 kWh kg^{-1} and 180 min. The BOD_5/COD ratio increased from 4.52×10^{-4} to 0.5573, confirming effluent biodegradability. These results suggest that EO can be considered as an efficient alternative for the mineralization of effluents coming from cyanide-involving industrial processes.

Acknowledgements The authors thank Universidad Nacional de Colombia—Sede Manizales (Proyecto HERMES-27797) for its financial support of this research. Guillermo Humberto Gaviria was a holder of a fellowship of COLCIENCIAS (Convocatoria Nacional Jóvenes Investigadores e Innovadores año 2014).

References

1. Kirk-Othmer (2002) Encyclopedia of chemical technology. Wiley, Hoboken
2. Mudder TI, Botz MM, Smith A (2001) Chemistry and treatment of cyanidation wastes. Mining Journal Books Ltd., London
3. U.S. Department of Health and Human Services (2006) Toxicological profile for Cyanide. https://www.atsdr.cdc.gov/toxprofiles/tp8.pdf. Accessed 02 July 2019
4. Akcil A (2003) Destruction of cyanide in gold mill effluents: biological versus chemical treatments. Biotechnol Adv 21:501–511
5. Dobrosz-Gómez I, Ramos García BD, Gil Pavas E, Gómez-García MÁ (2017) Kinetic study on HCN volatilization in gold leaching tailing ponds. Miner Eng 110:185–194. https://doi.org/10.1016/j.mineng.2017.05.001
6. Dash RR, Gaur A, Balomajumder C (2009) Cyanide in industrial wastewaters and its removal: a review on biotreatment. J Hazard Mater 163:1–11. https://doi.org/10.1016/j.jhazmat.2008.06.051
7. Ministerio de Ambiente y Desarrollo Sostenible (2015) Resolución 0631 de 2015. https://www.minambiente.gov.co/images/.../app/resoluciones/d1-res_631_marz_2015.pdf. Accessed 02 June 2019
8. EPA (2017) Laws and Regulations. https://www.epa.gov/laws-regulations Accessed 02 June 2019
9. Kuyucak N, Akcil A (2013) Cyanide and removal options from effluents in gold mining and metallurgical processes. Miner Eng 50:13–29. https://doi.org/10.1016/j.mineng.2013.05.027
10. Deveci H, Yazıcı EY, Alp I, Uslu T (2006) Removal of cyanide from aqueous solutions by plain and metal-impregnated granular activated carbons. Int J Miner Process 79:198–208. https://doi.org/10.1016/j.minpro.2006.03.002
11. Maulana I, Takahashi F (2018) Cyanide removal study by raw and iron-modified synthetic zeolites in batch adsorption experiments. J Water Process Eng 22:80–86. https://doi.org/10.1016/j.jwpe.2018.01.013
12. Dai X, Simons A, Breuer P (2012) A review of copper cyanide recovery technologies for the cyanidation of copper containing gold ores. Miner Eng 25:1–13. https://doi.org/10.1016/j.mineng.2011.10.002
13. Parga JR, Shukla SS, Carrillo-Pedroza FR (2003) Destruction of cyanide waste solutions using chlorine dioxide, ozone and titania sol. Waste Manag 23:183–191. https://doi.org/10.1016/S0956-053X(02)00064-8
14. Yeddou AR, Chergui S, Chergui A et al (2011) Removal of cyanide in aqueous solution by oxidation with hydrogen peroxide in presence of copper-impregnated activated carbon. Miner Eng 24:788–793. https://doi.org/10.1016/j.mineng.2011.02.012
15. Carrillo-Pedroza FR, Nava-Alonso F, Uribe-Salas A (2000) Cyanide oxidation by ozone in cyanidation tailings: reaction kinetics. Miner Eng 13:541–548. https://doi.org/10.1016/S0892-6875(00)00034-0
16. Akcil A, Mudder T (2003) Microbial destruction of cyanide wastes in gold mining: process review. Biotech Lett 25:445–450. https://doi.org/10.1023/A:1022608213814
17. Guamán MP, Nieto DA (2018) Evaluation of the rotational speed and carbon source on the biological removal of free cyanide present on gold mine wastewater, using a rotating biological contactor. J Water Process Eng 23:84–90. https://doi.org/10.1016/j.jwpe.2018.03.008
18. Malhotra S, Pandit M, Kapoor JC, Tyagi DK (2005) Photo-oxidation of cyanide in aqueous solution by the UV/H_2O_2 process. J Chem Technol Biotechnol 80:13–19. https://doi.org/10.1002/jctb.1127
19. Valiūnienė A, Baltrūnas G, Keršulytė V et al (2013) The degradation of cyanide by anodic electrooxidation using different anode materials. Process Saf Environ Prot 91:269–274. https://doi.org/10.1016/j.psep.2012.06.007
20. Abdel-Aziz MH, Bassyouni M, Gutub SA et al (2016) Removal of cyanide from liquid waste by electrochemical oxidation in a new cell design employing a graphite anode. Chem Eng Commun 203:1045–1052. https://doi.org/10.1080/00986445.2015.1135796
21. Bakir Öğütveren Ü, Törü E, Koparal S (1999) Removal of cyanide by anodic oxidation for wastewater treatment. Water Res 33:1851–1856. https://doi.org/10.1016/S0043-1354(98)00362-5
22. Felix-Navarro RM, Wai Lin S, Violante-Delgadillo V et al (2011) Cyanide degradation by direct and indirect electrochemical oxidation in electro-active support electrolyte aqueous solutions. J Mex Chem Soc 55:51–56
23. Pineda CA, Silva S (2007) Indirect electrochemical oxidation of cyanide by hydrogen peroxide generated at a carbon cathode. Int J Hydrogen Energy 32:3163–3169. https://doi.org/10.1016/j.ijhydene.2006.04.011
24. Iordache I, Nechita MT, Rosca I, Aelenei N (2004) Ultrasound assisted electrochemical degradation of cyanides: influence of electrode type. Turk J Eng Environ Sci 28:377–380
25. Rice EW, Baird RB, Eaton AD (2017) Standard Methods for the Examination of Water and Wastewater, 23rd Edition. American Water Works Association (AWWA, WEF and APHA), Washington, DC
26. GilPavas E, Dobrosz-Gómez I, Gómez-García MÁ (2017) Coagulation-flocculation sequential with Fenton or Photo-Fenton processes as an alternative for the industrial textile wastewater treatment. J Environ Manag 191:189–197. https://doi.org/10.1016/j.jenvman.2017.01.015

27. Bezerra MA, Santelli RE, Oliveira EP, Villar LS, Escaleira LA (2008) Response surface methodology (RSM) as a tool for optimization in analytical chemistry. Talanta 76:965–977. https://doi.org/10.1016/j.talanta.2008.05.019
28. Ferreira SLC, Bruns RE, Ferreira HS, Matos GD, David JM, Brandao GC, da Silva EGP, Portugal LA, dos Reis PS, Souza AS, dos Santos WNL (2007) Box-Behnken design: an alternative for the optimization of analytical methods. Anal Chim Acta 597:179–186. https://doi.org/10.1016/j.aca.2007.07.011
29. Montgomery D (2005) Design and analysis of experiments, 5th edn. Wiley, Hoboken
30. Zarei M, Niaei A, Salari D, Khataee A (2010) Application of response surface methodology for optimization of peroxi-coagulation of textile dye solution using carbon nanotube–PTFE cathode. J Hazard Mater 173:544–551. https://doi.org/10.1016/j.jhazmat.2009.08.120
31. Comninellis C, Cheng G (2010) Electrochemistry for the environment. Springer, New York
32. Zapata A, Malato S, Sanchez-Perez JA et al (2010) Scale-up strategy for a combined solar photo-Fenton/biological system for remediation of pesticide-contaminated water. Catal Today 151:100–106. https://doi.org/10.1016/j.cattod.2010.01.034

Affiliations

Izabela Dobrosz-Gómez[1] · Miguel Ángel Gómez García[2] · Guillermo H. Gaviria[2] · Edison GilPavas[3]

✉ Izabela Dobrosz-Gómez
idobrosz-gomez@unal.edu.co

[1] Grupo de Investigación en Procesos Reactivos Intensificados y Materiales Avanzados -PRISMA, Departamento de Física y Química, Facultad de Ciencias Exactas y Naturales, Universidad Nacional de Colombia, Sede Manizales, Campus La Nubia, km 9 vía al Aeropuerto la Nubia, Apartado Aéreo 127, Manizales, Caldas, Colombia

[2] Grupo de Investigación en Procesos Reactivos Intensificados y Materiales Avanzados - PRISMA, Departamento de Ingeniería Química, Facultad de Ingeniería y Arquitectura, Universidad Nacional de Colombia, Sede Manizales, Campus La Nubia, km 9 vía al Aeropuerto la Nubia, Apartado Aéreo 127, Manizales, Caldas, Colombia

[3] GIPAB: Grupo de Investigación en Procesos Ambientales, Departamento de Ingeniería de Procesos, Universidad EAFIT, Carrera 49 #7 sur 50, Medellín, Colombia